Early structure formation from cosmic string loops

Benjamin Shlaer[1], Alexander Vilenkin[1], Abraham Loeb[2]

[1]*Institute of Cosmology, Department of Physics and Astronomy, Tufts University, Medford, MA 02155, USA*

[2]*Harvard-Smithsonian Center for Astrophysics, 60 Garden Street, Cambridge, MA, 02138, USA*

Abstract

We examine the effects of cosmic strings on structure formation and on the ionization history of the universe. While Gaussian perturbations from inflation are known to provide the dominant contribution to the large scale structure of the universe, density perturbations due to strings are highly non-Gaussian and can produce nonlinear structures at very early times. This could lead to early star formation and reionization of the universe. We improve on earlier study of these effects by accounting for high loop velocities and for the filamentary shape of the resulting halos. With reasonable assumptions about the astrophysical parameters, the WMAP data impose a bound $G\mu < 10^{-7}$ (??) on the energy scale of cosmic strings. We also comment on other possible observational implications of early structure formation by strings.

I. INTRODUCTION

Cosmic strings are linear topological defects that could be formed at a phase transition in the early universe [1]. They are predicted in a wide class of particle physics models. Some superstring-inspired models suggest that fundamental strings may also have astronomical dimensions and play the role of cosmic strings [2–4].

Strings can be detected through a variety of observational effects. Oscillating loops of string emit gravitational waves – both bursts and a stochastic background. They can also be sources of ultrahigh-energy cosmic rays. Long strings can act as gravitational lenses [5–7] and can produce characteristic signatures in the CMB: discontinuous temperature jumps [8] along the strings and a B-mode polarization pattern due to rotational perturbations induced by strings. Formation and evolution of cosmic strings and their possible observational effects have been extensively discussed in the literature; for a review see, e.g., [9, 10].

The strength of gravitational interactions of strings is characterized by the dimensionless number $G\mu$, where μ is the mass per unit length of string and G is Newton's constant. Early work on cosmic strings was largely motivated by the idea that oscillating string loops and wakes formed by rapidly moving long strings could serve as seeds for structure formation. This scenario, which required $G\mu \sim 10^{-6}$, has been conclusively ruled out by CMB observations. Present CMB bounds constrain $G\mu$ to be less than about 2×10^{-7} [11–13]. A much stronger bound, $G\mu < 4 \times 10^{-9}$, has recently been claimed in [14] based on the millisecond pulsar observations of the gravitational wave background. (We shall argue in Sec. VI that this bound could be significantly relaxed, in the light of the latest string simulations.)

The CMB and other data are consistent with a Gaussian spectrum of density perturbations predicted by the theory of inflation; the contribution of strings, if any, can account for no more than 10% of the spectral power. This does not mean, however, that strings always played a subdominant role in structure formation. Density perturbations due to strings are highly non-Gaussian and can produce nonlinear structures at very early times. This could result in early star formation and reionization of the universe [15–19].

This and other effects of strings depend on the details of string evolution, which until recently remained rather uncertain. Early string simulations [20, 21] suggested that loops produced by the string network are very small and short-lived. Hence, it was assumed in Refs. [15–18] that the main effect on structure formation was due to long string wakes.

However, more recent, high-resolution simulations have demonstrated that a substantial fraction of the network energy goes into large loops, having length of about 5% of the horizon [22–24]. This pattern is established only after a long transient period dominated by very small loops; apparently it is this period that was observed in previous simulations. Ref. [19] studied structure formation and reionization in this new string evolution scenario and found that the resulting bound on $G\mu$ was competitive with the CMB and gravitational radiation bounds.

In the present paper we shall reexamine early structure formation by cosmic strings and its effect on the ionization history of the universe. An important fact not taken into account in Ref. [19] is that string loops are typically produced with high velocities: $v \sim 0.3$ for the largest loops and even higher for smaller ones [24]. Accretion on such rapidly moving loops is rather different from spherical accretion on a stationary point mass which was assumed in [19]. We also make use of the latest string simulations which yielded more reliable results for the size and velocity distributions of cosmic string loops.

The paper is organized as follows. In the next section we review the evolution of cosmic strings and introduce the relevant loop distributions. In Sec. III we study accretion of matter onto a moving loop, first treating the loop as a point mass and then accounting for its finite size (which turns out to be significant). We find that loop seeded halos have the form of highly elongated filaments which then fragment into smaller "beads". The resulting halo spectrum is calculated in Sec. IV. The reionization history and observational constraints on the string parameter $G\mu$ are discussed in Sec. V. Our results are summarized and discussed in Sec. VI. In the Appendix we discuss the "rocket effect" – the self-acceleration of string loops due to asymmetric emission of gravitational waves – and show that it is not significant for structure formation.

II. COSMIC STRING EVOLUTION

A. Long strings

An evolving network of cosmic strings consists of two components: long strings and sub-horizon closed loops. The long string component evolves in a scaling regime in which the typical distance between the strings and all other linear measures of the network remain at

a constant fraction of the horizon size $d_{\rm h}(t)$. This dynamic is maintained by the production of loops via reconnection at string intersections, and subsequent evaporation of loops by gravitational radiation. On super-horizon length scales, long strings have the form of random walks, while on smaller scales they exhibit a wide spectrum of wiggles and kinks, which are remnants of the initial wiggliness of the network and of earlier reconnections. These small-scale features are gradually smoothed out by expansion and by gravitational radiation back-reaction.

The total energy density in the long ("infinite") strings can be expressed as

$$\rho_\infty = \mu/(\gamma d_{\rm h})^2 \tag{1}$$

where μ is the mass per unit length of string (equal to the string tension), the radiation era horizon distance is $d_{\rm h} = 2t$, γ is a constant coefficient, and the quantity $\gamma d_{\rm h}$ defines the average inter-string distance. The idea that the network properties are determined by the horizon distance alone is known as the scaling hypothesis [1, 25]; for the long string component it has been confirmed through numerical simulations [20, 21, 26].

The coefficient γ in (1) depends on the reconnection probability $p_{\rm rec}$ of intersecting strings. For "ordinary" particle physics strings, $p_{\rm rec} = 1$ and simulations give $\gamma \approx 0.15$ in the radiation era. For cosmic superstrings, the reconnection probability is expected to be much smaller, $0.1 \gtrsim p_{\rm rec} \gtrsim 10^{-3}$ [27], resulting in a smaller value of γ and a denser string network. Simple arguments suggest that $\gamma \propto p_{\rm rec}^{1/2}$ [28, 29], but simulations indicate a weaker dependence [30]. Here we shall focus on ordinary strings with $p_{\rm rec} = 1$.

B. Loop distribution: a simple model

The length distribution of loops produced by the network (the so-called loop production function) obtained in recent simulations has a double-peak structure, indicating two different populations of loops. First, there is a scaling loop distribution, with a typical loop length of about 5% of the horizon and a wide tail extending to smaller scales. And then there is a non-scaling distribution of very small loops with sizes comparable to the initial scale of the network at formation. The hight of the non-scaling peak is observed to decrease somewhat in the course of the simulation, with the extra power contributing to the short-length tail of the scaling peak. One might expect that the non-scaling peak will eventually disappear

[22–24], but Ref. [31] argued that it could also survive at late times. In the latter case, the asymptotic double-peak loop distribution will still scale, but the typical loop size in the short-length peak will be set by the gravitational radiation damping.

At present one can only guess which of the two options will be supported by future simulations, but fortunately this is not important for the purposes of the present paper. The non-scaling loops are highly relativistic, with the dominant part of their energy being kinetic energy. This energy redshifts with the expansion and has very little effect on the gravitational clustering. The same applies to loops in the tail of the scaling distribution. Only loops near the peak of the scaling distribution, which are formed with mildly relativistic velocities, are relevant for structure formation. Moreover, halos formed by small loops at the tail of the distribution have small virial velocities. This inhibits cooling and star formation in such halos.

The string loops of interest to us here will be those which formed during the radiation era but have not yet decayed at $t_{\rm eq}$. The energy density of loops that were chopped off the network in one Hubble time is comparable to the energy density of long strings. However, the loop energy redshifts like matter, while the long string energy redshifts like radiation. So, if loops are long and live much longer than a Hubble time, they dominate the energy of the network and play dominant role in structure formation.

Using energy conservation, the power flowing into loops per unit physical volume during the radiation era must obey

$$\dot{\rho}_{\rightarrow \rm loops} = \frac{1-\langle v_\infty^2\rangle}{t}\rho_\infty = \frac{\mathcal{P}\mu}{d_h^3}, \tag{2}$$

where $\langle v_\infty^2\rangle$ is the mean square velocity of the long strings. Simulations give $\langle v_\infty^2\rangle \approx 0.4$ and $\mathcal{P} := \mu^{-1} d_h^3 \dot{\rho}_{\rightarrow \rm loops} \approx 50$ in this epoch. Neglecting (for the time being) the center-of-mass loop velocity, the comoving number density distribution of loops $n(t,m)$ should satisfy

$$\frac{1}{a^3(t)}\frac{d}{dt}\left(\int_0^\infty n(t,m) m dm\right) = \dot{\rho}_{\rightarrow loops}. \tag{3}$$

Since we are only interested in loops near the peak of scaling distribution, it is a reasonable approximation to assume that all relevant loops are formed having length equal to a fixed fraction of the horizon size. Hence, we set the loop mass at formation to be

$$m = \alpha \mu d_{\rm h} \tag{4}$$

with $\alpha \approx 0.05$. The distribution of such loops obeys

$$\frac{1}{a^3(t)}\frac{d}{dt}\left[n(t,m)m\right] = \delta(m - 2\mu\alpha t)\frac{\delta\mathcal{P}\mu}{8t^3}, \tag{5}$$

and so

$$n(t,m) = \frac{a^3(\frac{m}{2\mu\alpha})}{m}\frac{\delta\mathcal{P}\mu}{8\left(\frac{m}{2\mu\alpha}\right)^3 2\mu\alpha} = \frac{\sqrt{\alpha}\mu^{3/2}\delta\mathcal{P}}{4\sqrt{2}m^{5/2}t_{eq}^{3/2}} \qquad \text{for } m \leq 2\mu\alpha t \tag{6}$$

and $n(t,m) = 0$ otherwise. Here, $\delta\mathcal{P} \approx 5$ reflects the fact that the effective power flowing into these large loops is about ten percent of the total power $\mathcal{P} \approx 50$, as suggested by simulations [24]. We have also used $a(t) = (t/t_{eq})^{1/2}$, normalizing to $a(t_{eq}) = 1$.

The apparent divergence of loop mass density $m\,n(t,m)dm$ at small m is absent if we include the decay of loops due to gravitational radiation, $\dot{m} \approx -\Gamma G\mu^2$, with $\Gamma \approx 50$. This correction is only significant for very small loops.

C. Incorporating loop speed

We now perform a more precise calculation which includes finite velocity effects, which are significant. We characterize the number density of loops by their mass m and speed v. All quantities will be expressed per comoving volume from here onward. The comoving number density of cosmic string loops with mass between m and $m + dm$ and with speed between v and $v + dv$ is given by $n(t,m,v)dv\,dm$. The loop production function is $g(t,m,v)dt\,dv\,dm$, the number of such loops per comoving volume produced by the cosmic string network between time t and $t + dt$. The redshifting of loop speeds is given by $\dot{v} \approx -Hv$ where $H = \dot{a}/a = 1/(2t)$ is the Hubble rate, and we are assuming non-relativistic v, which is justified for the subset of loops which contribute to star formation.

We can integrate the production rate to find the number density per comoving volume,

$$n(t,m,v) \;=\; \int_0^t dt' g(t',m',v')\frac{\partial m'}{\partial m}\frac{\partial v'}{\partial v}. \tag{7}$$

This states that the number of loops of mass m and speed v at time t is the integral of the production rate of loops over all prior times $t' \leq t$, where the relevant production is of loops which will eventually have mass m and speed v. Hence the first step is to write down the

solution to the flow, namely

$$m'(t';m,t) \approx m + \Gamma G\mu^2(t-t'), \tag{8}$$

$$v'(t';v,t) \approx v\frac{a(t)}{a(t')}. \tag{9}$$

These tell us e.g., what speed v' a loop must have at production time t' in order for it to have a speed v at time t. The Jacobian factor $\frac{\partial v'}{\partial v}$ captures the changing size of the volume element dv. The same applies to m as well. We are neglecting the effects on v of anisotropy in the loop gravitational radiation, also known as the "rocket effect", which causes the loops to accelerate as they evaporate. This will be justified in the Appendix.

The energy of a loop is given by $m/\sqrt{1-v^2}$, and so using Eq. (2),

$$\frac{\mathcal{P}\mu}{d_{\rm h}^3(t)} = \int_0^\infty \int_0^1 \frac{m}{\sqrt{1-v^2}} \frac{g(t,m,v)}{a^3(t)} dv\, dm. \tag{10}$$

Since all quantities of interest are linear in g, we can maintain generality while treating g as a delta-function source, i.e.,

$$g(t,m,v) = \frac{a^3(t)\delta\mathcal{P}\mu\sqrt{1-v^2}}{d_{\rm h}^3(t)m}\delta\left(m-\alpha\mu d_{\rm h}(t)\right)\delta\left(v-\alpha_v\right), \tag{11}$$

where in this form we can imagine taking the values suggested by simulations, namely

$$\alpha = 0.05, \quad \alpha_v = 0.3, \quad \delta\mathcal{P} = 5. \tag{12}$$

The results using the actual loop production function, including small relativistic loops, can always be obtained by integrating any expression involving $\delta\mathcal{P}$ with the replacement $\delta\mathcal{P} \to xf(x,p)dx\,dp$, where $x = \alpha/\sqrt{1-v^2}$, $p = v/\sqrt{1-v^2}$, and $f(x,p)$ is the loop-production function following the definitions in [24]. Because of this substitution possibility, we will refer to Eq. (11) as the delta-function form of g, and Eq. (12) as the delta-function approximation for g.

Combining the equations of this section, the comoving loop number density is

$$\begin{aligned} n(t,m,v) &= \int_0^t dt' g(t',m',v')\frac{\partial m'}{\partial m}\frac{\partial v'}{\partial v}, \\ &= \int_0^t dt' \frac{a^3(t')\delta\mathcal{P}\mu}{d_{\rm h}^3(t')m'}\delta\left(m'-\alpha\mu d_{\rm h}(t')\right)\delta\left(v'-\alpha_v\right)\frac{a(t)}{a(t')}, \\ &\approx \frac{\sqrt{\alpha}\delta\mathcal{P}\mu^{3/2}\delta\left(v-\sqrt{\frac{m}{2\alpha\mu t}}\alpha_v\right)}{4\sqrt{2}\left(m+\Gamma G\mu^2 t\right)^{5/2}t_{\rm eq}^{3/2}(t)}. \end{aligned} \tag{13}$$

III. ACCRETION ONTO A COSMIC STRING LOOP

As we explained in Section II.B, the dominant loop energy density will always be from loops produced in the radiation era. This is because the integrated power flowing into loops scales like $1/t^2$, whereas the subsequent dilution only scales like $1/a^3$. Thus in the radiation-era (when $a \sim t^{1/2}$), loops pile up from early times. This growth is cut off by loop evaporation to gravitational radiation, which is a slow process for low tension strings. So structure formation is mainly sensitive to radiation-era loops which have survived to the time of matter domination.

Of particular interest are halos which become large enough for stars to form [32]. This requires the baryons to collapse to sufficient density, which can only happen due to dissipation. When the neutral hydrogen atoms have large enough virial velocity, collisions will have sufficient center-of-mass energy to excite their electrons and radiate. The energy escaping with the radiated photons ensures that the hydrogen loses gravitational potential energy. This cooling moves the hydrogen toward the center of the halo. The critical virial temperature for efficient cooling T_* can be as low as 200K in the case of molecular hydrogen, but we will neglect this mechanism since the molecule is too fragile to survive UV light from the very first stars. Instead, we will consider two possible values, 10^4K and 10^3K, below which star formation does not occur[1]. Because the virial temperature is proportional to a positive power of the halo mass, which is proportional to the seed (loop) mass, there is a minimum loop size which can lead to star formation. We can conclude that early stars can only come from loops produced late enough to have this size. We will denote the minimum scale factor after which star-forming loops can be produced by a_i^*, which we will now estimate. Throughout, we define the scale factor at matter-radiation equality to be unity, $a(t_{\rm eq}) = 1$.

[1] Because of the relative motion between the baryon and dark matter fluid, smaller halos will not lead to significant star formation [33, 34].

A. Spherical accretion

For a spherical halo of mass M formed at redshift z, the virial temperature is given by [32]

$$T_{\rm vir} = 10^4 \left(\frac{M}{10^8 M_\odot}\right)^{2/3} \left(\frac{1+z}{10}\right) {\rm K}, \tag{14}$$

and so the minimal mass of a halo that has $T_{vir} \geq 10^4$ K at z is

$$M_*(z) = 3 \times 10^9 M_\odot (1+z)^{-3/2} \left(\frac{T_*}{10^4 {\rm K}}\right)^{3/2}. \tag{15}$$

Because the vast majority of loops are moving rather quickly, the more appropriate bound on production time considers elongated filaments, rather than spherical halos. Elongated halo filaments have a virial temperature [**?**] dependent entirely on their linear mass density $\mu_{\rm fil}$, which we will calculate below. These filaments will later collapse into beads, which subsequently merge into larger beads, but this process does not significantly affect the virial temperature.

B. Accretion onto a moving point mass

If we assume the loop is non-relativistic and has velocity $v_{\rm eq} > 0$ in the $+y$-direction at $t_{\rm eq}$, its subsequent velocity is given by

$$v(a) = \frac{v_{\rm eq}}{a}, \tag{16}$$

where $a = (t/t_{\rm eq})^{2/3}$. The trajectory in comoving coordinates is then

$$y(a) = 3 v_{\rm eq} t_{\rm eq} \left(1 - \frac{1}{\sqrt{a}}\right). \tag{17}$$

Using our delta-function loop production function, the loop velocity at equality is

$$v_{\rm eq} \approx \alpha_v a_i, \tag{18}$$

where $a_i < 1$ is the scale factor at loop production, relative to $a_{\rm eq} = 1$.

Given a point mass in the above trajectory, we can find the cylindrically symmetric turn-around surface by considering a particle at comoving initial location $(x_0, y_0, 0)$. (Here we closely follow the analysis in [35].) Let us label the moment of closest approach of the mass

by the scale factor a_0, i.e., the loop trajectory $y(a)$ obeys $y(a_0) = y_0$. Using the impulse approximation, the velocity kick on the particle due to the passing point mass is

$$v_x \sim \frac{Gm}{(a_0 x_0)^2}\Delta t_0 \sim \frac{Gm}{a_0 x_0 v(a_0)}, \tag{19}$$

where

$$\Delta t_0 \sim \frac{a_0 x_0}{v(a_0)}. \tag{20}$$

This particle will then be displaced after one subsequent Hubble time $H_0^{-1} \sim t_{\rm eq} a_0^{3/2}$ by an amount

$$a_0 \Delta x_0 \sim v_x t_{\rm eq} a_0^{3/2}, \tag{21}$$

and so the corresponding density perturbation is

$$\delta_0 \sim \frac{\Delta x_0}{x_0} \sim \frac{Gm t_{\rm eq}}{x_0^2 v(a_0) a_0^{1/2}}, \tag{22}$$

which grows to be

$$\delta(a) \sim \delta_0 \frac{a}{a_0} \sim \frac{Gm t_{\rm eq} a}{x_0^2 v(a_0) a_0^{3/2}}. \tag{23}$$

The turnaround surface is given by $\delta(a) \sim 1$, so the profile of the collapsed region from a passing point mass with arbitrary velocity $v(a_0)$ is

$$x_{\rm ta}^2(a_0, a) \sim \frac{Gm t_{\rm eq} a}{v(a_0) a_0^{3/2}}, \tag{24}$$

where the time dependence is in $a = (t/t_{\rm eq})^{2/3}$, and the y-dependence is in $a_0(y_0)$ via Eq. (17) with $y(a_0) = y_0$. Notice $a \geq a_0$, since the turnaround surface extends only behind the loop's y-position. The halo mass is then given by the total mass inside the turnaround surface

$$\begin{aligned} M(t) &= \rho a^3(t) \int_0^{y(a(t))} \pi x_{\rm ta}^2(a_0(y_0), a(t)) dy_0 = \rho a^3(t) \int_{t_{\rm eq}}^{t} \pi x_{\rm ta}^2 \frac{dy(a(t_0))}{dt_0} dt_0 \\ &= \rho a^3(t) \int_{t_{\rm eq}}^{t} \frac{\pi x_{\rm ta}^2 v(a_0)}{a_0} dt_0 = \frac{1}{6\pi G t_{\rm eq}^2} \int_{t_{\rm eq}}^{t} \frac{\pi G m t_{\rm eq} a(t)}{a_0^{5/2}} dt_0 = \frac{m a(t)}{6} \int_{t_{\rm eq}}^{t} \frac{t_{\rm eq}^{2/3}}{t_0^{5/3}} dt_0 \\ &= \frac{m}{4}\left[a(t) - 1\right]. \end{aligned} \tag{25}$$

Interestingly, the loop trajectory does not affect the halo mass at this level of approximation. A more accurate analysis by Bertschinger [35], using the Zel'dovich approximation, gives $M(t) = \frac{3}{5} m a(t)$. We will simply use

$$M(t) \sim m a(t). \tag{26}$$

We can solve for the shape and size of the turnaround surface by combining Eqs. (16, 17 & 24). This gives

$$x_{\rm ta}(y,a) = t_{\rm eq}\sqrt{\frac{2\alpha G\mu a_i a}{\alpha_v}\left(1-\frac{y}{3\alpha_v a_i t_{\rm eq}}\right)} \qquad \text{for} \quad 0 \le y \le 3\alpha_v a_i t_{\rm eq}\left(1-\frac{1}{\sqrt{a}}\right). \quad (27)$$

Notice that these halos are very elongated: the eccentricity after a Hubble time is given by

$$\left.\frac{y}{x_{\rm ta}}\right|_{a\sim 2} \approx \frac{\alpha_v^{3/2} a_i^{1/2}}{\sqrt{\alpha G\mu}} \sim 10^3. \quad (28)$$

Here we have assumed $a_i = \sqrt{t_i/t_{\rm eq}} \sim 0.1$, $G\mu \sim 10^{-8}$, and used the delta-function approximation $\alpha_v \sim 0.3$ and $\alpha \sim 0.05$. We will now refer to these elongated structures as filaments. Halos will form from linear instabilities of the filaments.

In this discussion we disregarded the so-called rocket effect – the self-acceleration of the loop due to asymmetric emission of gravitational waves. This has negligible effect on the loop's velocity, except toward the end of the loop's life, when the loop can be accelerated to a mildly relativistic speed, $v \lesssim 0.1$. The loop trajectory with the rocket effect included is discussed in the Appendix, where it is shown that the rocket acceleration has little influence on halo formation.

C. Accretion onto a finitely extended loop

Since the loop has a finite radius $R = \beta m/\mu$, with $\beta \sim 0.1$, only the matter outside this distance will feel a momentum kick from the passing loop[2]. We should then only consider the portion of the turnaround surface where

$$x_{\rm ta} > R/a_0, \quad (29)$$

or using Eqs. (16 & 24),

$$\alpha_v \frac{a_i}{a_0} < \frac{G\mu a a_0^{1/2}}{2\beta^2\alpha a_i^2}, \quad (30)$$

[2] The rapidly oscillating string will leave wakes of overdensity behind the fast segments, i.e., even inside the loop radius R. We neglect this effect, since only a small fraction $\sim 8\pi G\mu/v$ of the material is affected, and the wakes are probably too thin to allow star formation.

where again, a_0 should be thought of as a measure of the y-coordinate given by $y_0 = y(a_0)$ above. This equation is a restriction on the validity of the turnaround surface Eq. (27); in places where the turnaround surface is smaller than the loop radius, it does not exist and so should be thought of as ending rather than closing.

For the faster loops (whose turnaround surfaces have smaller physical radius c.f. Eq. (24)), the loop radius will entirely cloak the turnaround surface at the onset of matter domination. Because the turnaround surface radius grows relative to the comoving loop radius, there will eventually be a time when the surface emerges. The surface will emerge as a hoop surrounding the loop, which grows into a cylinder. The front of the cylinder will move forward with the loop, and continue to grow in diameter with expansion. The back of the cylinder will extend back to the location where the turnaround surface is smaller than the comoving loop radius. Eventually the back of the cylinder will reach $y = 0$, i.e., the location of the loop at the onset of matter domination.

We can now talk of three distinct phases of loop-seeded filaments in the matter era. The early type are those which are not accreting, because no part of the turnaround surface has emerged from behind the loop radius. The late type are filaments whose entire turnaround surface is larger than the loop radius. Because the point-mass approximation holds in this case, the total filament mass is given by Eq. (26). We will call these "normal growth" filaments. The intermediate type of filament are those whose turnaround surfaces are growing both in the positive y-direction with the loop motion, as well as in the negative y-direction as more and more of the turnaround surface emerges from beneath the loop radius. We will call these "accelerated growth" filaments, since they are catching up from having zero mass to eventually have normal mass.

We can find when the turnaround surface first emerges from behind the loop radius R by setting $a_0 = a$ in Eq. (30) to find

$$a > a_{\rm min} = \left(\frac{2\beta^2\alpha\alpha_v a_i^3}{G\mu}\right)^{2/5}. \tag{31}$$

The turnaround surface stops its accelerated growth when Eq.(30) is satisfied all the way back to $y_0 = 0$, i.e. $a_0 = 1$, and so the normal-growth regime for the filament takes over after

$$a > a_{\rm max} = \left(\frac{2\beta^2\alpha\alpha_v a_i^3}{G\mu}\right) = a_{\rm min}^{5/2}. \tag{32}$$

The turnaround surfaces for $a = 2, 3...40$ are shown in Fig. 1.

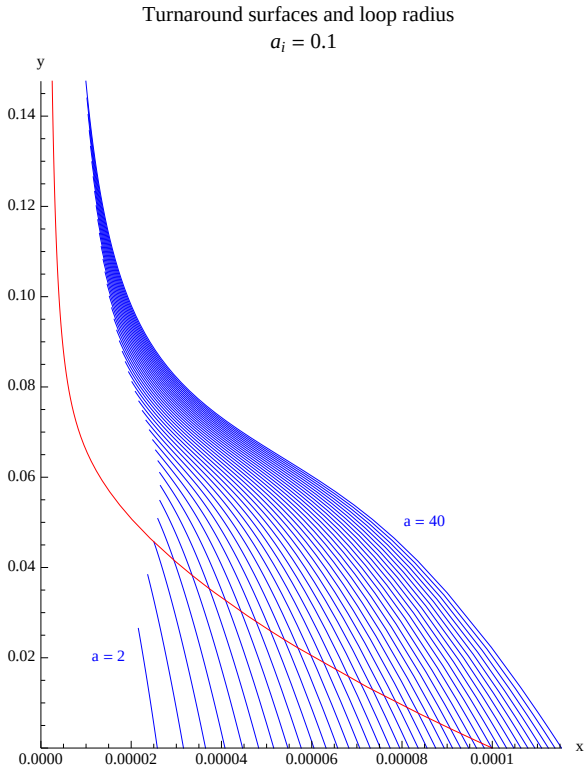

FIG. 1: Time-lapse illustration of comoving turnaround surfaces (blue) for a loop of tension $G\mu = 10^{-8}$. The comoving loop extension is shown in red. Notice the aspect ratio is reduced by a factor of 1000:1, and units are $t_{\rm eq}$. We can read off $a_{\rm min} \approx 4, a_{\rm max} \approx 30$ from the figure. We use $a_i = 0.1$ and the delta-function approximation parameters of Eq. (12) to determine the mass and speed of the loop. We have included the rocket effect for completeness (but see Appendix).

Given these turnaround surfaces, the total filament mass can be shown to be

$$M_{\rm fil}(t) \quad = \quad \rho_{\rm eq} \int_{y_0^{\rm min}(t)}^{y(t)} x(t)_{\rm ta}^2 dy_0 \quad \sim \quad \begin{cases} 0 & a < a_{\rm min} \\ m(\frac{a^{5/3}}{a_{\rm min}^{5/3}} - 1) & a_{\rm min} < a < a_{\rm max} \\ m(a-1) & a_{\rm max} < a \end{cases} \tag{33}$$

Note that since $a_{min}^{5/3} \propto a_i^2 \propto m$, the filament mass in the accelerated growth regime is the same for all loops, independently of their mass m.

With the loop trajectory from Eq. (17), the physical length of the filament is given by

$$L_{\rm fil} \sim \begin{cases} 0 & a < a_{\rm min} \\ 3\alpha_v a_i t_{\rm eq}(\frac{a^{4/3}}{a_{\rm min}^{5/6}} - \sqrt{a}) & a_{\rm min} < a < a_{\rm max} \\ 3\alpha_v a_i t_{\rm eq}(a - \sqrt{a}) & a_{\rm max} < a \end{cases} \tag{34}$$

where $a_{\rm max} = a_{\rm min}^{5/2}$. This results in a linear mass density

$$\mu_{\rm fil} \sim \frac{M_{\rm fil}}{L_{\rm fil}} \sim \frac{2\alpha\mu a_i}{3\alpha_v}. \tag{35}$$

The corresponding virial temperature is found in [40] to be $T_{\rm vir} \approx \frac{1}{2} m_p G \mu_{\rm fil}$, where the proton mass $m_p = 1.1 \times 10^{13}$ K. Hence

$$T_{\rm vir} \sim \frac{G m_p \sqrt{m\alpha\mu}}{3\sqrt{2}\alpha_v t_{\rm eq}^{1/2}} \tag{36}$$

$$\sim 10^4 a_i \mu_{-8} \left(\frac{\alpha}{0.05}\right) \left(\frac{0.3}{\alpha_v}\right) {\rm K}. \tag{37}$$

Thus star formation occurs only for loops formed after

$$a_i^* \sim \frac{1}{\mu_{-8}} \left(\frac{0.05}{\alpha}\right) \left(\frac{\alpha_v}{0.3}\right) \left(\frac{T_*}{10^4 {\rm K}}\right). \tag{38}$$

Thus if $T_* = 10^4$K and the string tension $G\mu = 10^{-8}$ and below, star formation can only be attributed to loops in the low-velocity tail of the loop production function, which is highly suppressed.

If we restrict our attention to the ionization history of the universe, which is sensitive only to the total fraction of baryons in stars, we can neglect the subsequent dynamics of the filaments, which will fragment into beads which subsequently merge. This process will not significantly increase the virial temperature, since the filament is already in (2D) virial equilibrium, and the collapse into beads preserves the total energy.

D. Longitudinal filament collapse (or lack thereof)

Although we will find a linear instability of filaments toward collapse into bead-like halos, we can rule out the merging of the entire filament into a single large halo for all but the slowest loops. Here we consider the longitudinal collapse mode of the entire filament.

To show such a filament will not collapse, we can disregard the finite size of the loop, since accounting for the finite size can only further delay collapse. Then within a Hubble time of $t_{\rm eq}$ the filament mass is roughly the mass of the loop,

$$M_{\rm fil} \sim \alpha \mu t_i. \tag{39}$$

The length of the filament at this time is $L_{\rm fil} \sim v_{\rm eq} t_{\rm eq}$, and it grows with the scale factor as

$$L_{\rm fil} \sim v_{\rm eq} t_{\rm eq} a, \tag{40}$$

where the loop velocity at $t_{\rm eq}$ is $v_{\rm eq} \sim \alpha_v a_i$. The average mass per unit length is

$$\mu_{\rm fil} \sim \frac{M_{\rm fil}}{L_{\rm fil}} \sim \frac{\alpha \mu a_i}{\alpha_v}. \tag{41}$$

Let us first disregard the collapse along the filament axis. Then, at $t > t_{\rm eq}$, both the mass of the filament and its length grow like $(t/t_{\rm eq})^{2/3}$, so $\mu_{\rm fil}$ remains constant.

Now let us estimate the time scale of the longitudinal collapse. The characteristic longitudinal velocity that parts of the filament develop in a Hubble time t due to the filament's self-gravity is

$$v \sim (G\mu_{\rm fil}/L_{\rm fil}) t. \tag{42}$$

The collapse sets in when this becomes comparable to the Hubble velocity, $v_H \sim L/t$. This gives the following estimate for the redshift of the collapse:

$$(1+z) \sim \alpha G \mu \alpha_v^{-3} (t_{\rm eq}/t_i)^{1/2} (1 + z_{\rm eq}). \tag{43}$$

With $\alpha \sim 0.05$, $\alpha_v \sim 0.3$, $G\mu \lesssim 10^{-7}$ and $t_i/t_{\rm eq} \gtrsim 10^{-4}$, we get $1 + z < 1$, i.e., no collapse. This means that the filaments from cosmic string loops remain elongated by a large factor.

E. Fragmentation of filaments into beads

As the filaments grow in mass and thickness from radial infall of dark matter (and baryons after recombination), the longitudinal expansion maintains their linear mass density at a constant (in time) value $\mu_{\rm fil}(y) = \rho_{\rm eq} x_{\rm ta}^2(y, a)/a$. This overdense cylinder will be unstable to collapse into beads on scales longer than the Jeans length. The fastest growing instability was found in [36] to have a comoving wavelength $\lambda_{\rm J} \sim 4\pi x_{\rm vir}$, where the virial radius of

a cylindrically symmetric self gravitating gas is $x_{\rm vir} = x_{\rm ta}/\sqrt{e} \approx x_{\rm ta}$, and so the comoving length of the typical bead is comparable to the transverse dimension of the cylinder,

$$\Delta y \sim 4 x_{\rm ta}. \tag{44}$$

Longer wavelength instabilities represent merging of such beads, and occur on scales up to an order of magnitude longer. Since we characterize the beads by the size of the longest unstable mode, the length of the bead after merging is

$$L_{\rm bead} \approx 10 a \Delta y \approx 20\pi t_{\rm eq} \sqrt{\frac{a^3 a_i \alpha G\mu}{\alpha_v}} \approx 4 \times 10^{-5} \sqrt{a^3 a_i \mu_{-8}}\ {\rm Mpc}. \tag{45}$$

Because these are linear instabilities of high density regions, they grow quickly [**?**]. The number of beads is then

$$\nu_{\rm beads} = \frac{L_{\rm fil}}{L_{\rm bead}}. \tag{46}$$

In accelerated growth filaments, the bead mass is

$$M = \frac{M_{\rm fil}}{\nu_{\rm beads}} \approx 30 \alpha^{7/6} \beta^{-2/3} \sqrt{a_i} M_{\rm eq} \left(\frac{a G\mu}{\alpha_v} \right)^{11/6}, \tag{47}$$

where $M_{\rm eq} = t_{\rm eq}/G = 3.6 \times 10^{17} M_\odot$ is (roughly) the mass contained in a sphere of a horizon diameter at $t_{\rm eq}$.

The mass of each halo from normal-growth filaments can likewise be estimated to be

$$M \ = \ \frac{M_{\rm fil}}{\nu_{\rm beads}} \approx 36 M_{\rm eq} \left(\frac{G\mu\alpha a_i a}{\alpha_v} \right)^{3/2}. \tag{48}$$

By requiring $T_{\rm vir} \geq T_*$, we can set the lower bound on the bead mass at time $a(t)$ to be

$$M_* \approx 50 a^{11/6} t_{\rm eq} \sqrt{\frac{T_*}{m_p}} \left(\frac{\alpha^2 G \mu^4}{\alpha_v^4 \beta^2} \right)^{1/3} \tag{49}$$

for beads in accelerated growth filaments and

$$M_* \approx 200 M_{eq} a^{3/2} \left(\frac{T_*}{m_p} \right)^{3/2} \tag{50}$$

for beads in normal growth filaments.

IV. HALO SPECTRUM

We are interested in comparing models with cosmic strings of tension $G\mu = 10^{-8}\mu_{-8}$ with the standard structure formation scenario. The halo spectrum of the standard scenario is well approximated by the Sheth-Tormen mass function [39]. The $\Lambda_{\rm CDM}$ cosmology we use assumes the values of WMAP + BAO $+H_0$ [41] which for our purposes is just $z_{\rm eq} = 3232$ and $t_{\rm eq} = 1.73 \times 10^{-2}$Mpc. Because we are interested in early star formation, we will assume the growth function $D(z)$ scales simply as $D(z) \propto (1+z)^{-1}$.

We can calculate the spectrum of halos using the continuity equation. As we only consider radiation-era loops, there is no source term, since every loop already exists by $a = a_{\rm eq} = 1$, and subsequently is associated with one filament, which in turn is associated with some number $\nu_{\rm beads}$ of halos.

The spectrum of halos $N(M, a)$ at any redshift $z = \frac{z_{\rm eq}+1}{a} - 1$ is determined entirely from the spectrum of loops $n(a, m, v)$ at $a = a_{\rm eq}$ via

$$N(a, M) = \int \nu_{\rm beads}(a, m, v_{\rm eq}) n(a_{\rm eq}, m, v_{\rm eq}) \frac{\partial m}{\partial M} dv_{\rm eq}, \tag{51}$$

where

$$\nu_{\rm beads}(a, m, v_{\rm eq}) = \begin{cases} 0.08 v_{\rm eq}^{7/6} \left(\frac{M_{\rm eq}}{m}\right)^{5/6} \left(\frac{G\mu}{\beta}\right)^{2/3} a^{-1/6} & a_{\rm min} < a < a_{\rm max} \\ 0.08 \left(\frac{M_{\rm eq} v_{\rm eq}^3}{ma}\right)^{1/2} & a_{\rm max} < a, \end{cases} \tag{52}$$

$$n(a_{\rm eq}, m, v_{\rm eq}) \;=\; \frac{\delta \mathcal{P} \mu^{3/2} \sqrt{\alpha}\, \delta\!\left(v_{\rm eq} - \alpha_v \sqrt{\frac{m}{2\alpha\mu t_{\rm eq}}}\right)}{2(2t_{\rm eq})^{3/2} \left(m + \Gamma G\mu^2 t_{\rm eq}\right)^{5/2}}, \tag{53}$$

and $m(a; M)$ is given by combining Eqs. (47) or (48) with the substitution

$$a_i = \left(\frac{m}{2\alpha\mu t_{\rm eq}}\right)^{1/2}. \tag{54}$$

The delta-function enables us to integrate Eq. (51), yielding $v_{\rm eq} = \alpha_v (m/2\alpha\mu t_{\rm eq})^{1/2}$. We can neglect the correction proportional to Γ, since loops affected are too small to seed halos with $T_{\rm vir} \geq T_*$.

The Jacobian $(\partial m/\partial M)$ can be found from the loop mass

$$m(M) = \begin{cases} 3.0 \times 10^{-6} \frac{M^4}{M_{\rm eq}^3} \frac{G\mu}{\beta} \left(\frac{\beta \alpha_v^2}{\alpha (G\mu)^2 a^2}\right)^{11/3} & a_{\rm min} < a < a_{\rm max} \\ 1.7 \times 10^{-2} \frac{\alpha_v^2 M}{\alpha G\mu a^2} \left(\frac{M}{M_{\rm eq}}\right)^{1/3} & a_{\rm max} < a. \end{cases} \tag{55}$$

Note that although $m(M)$ is continuous at the transition between the accelerated and normal growth regimes at $a = a_{max}$, the derivative $(\partial m/\partial M)$ is not, resulting in a discontinuity in the halo spectrum (51).

We can write $a_{\rm min}$ and $a_{\rm max}$ from Eq. (32) without reference to a_i by using Eq. (54),

$$a_{\rm max} = \frac{\beta^2\alpha_v}{\sqrt{2\alpha}(G\mu)^{5/2}}\left(\frac{m}{M_{\rm eq}}\right)^{3/2}, \tag{56}$$

$$a_{\rm min} = a_{\rm max}^{2/5}. \tag{57}$$

We can also express $a_{\rm max}$ in terms of the halo mass M by substituting the lower expression in (55) with $a = a_{\rm max}$ into (56) and then solving for $a_{\rm max}$. This gives

$$a_{\rm max} = \frac{0.2\alpha_v}{G\mu}\left(\frac{\beta M}{\alpha M_{\rm eq}}\right)^{1/2} = \frac{0.014}{\mu_{-8}}\left(\frac{M}{M_\odot}\right)^{1/2}. \tag{58}$$

The halo spectrum is then given by

$$N(a,M) = \begin{cases} N_{\rm acc}(a,M) & a < a_{\rm max} \\ \\ N_{\rm norm}(a,M) & a > a_{\rm max}, \end{cases} \tag{59}$$

where

$$N_{\rm acc}(a,M) = 1.7\times 10^8\frac{\alpha_v\beta\delta\mathcal{P}}{G^3M^4}\left(\frac{M_{\rm eq}}{M}\right)^4\left[\frac{\alpha}{\alpha_v^2\beta}(G\mu a)^2\right]^{19/3}, \tag{60}$$

$$N_{\rm norm}(a,M) = \frac{1.8\alpha\delta\mathcal{P}}{\alpha_v G^3M^4}\left(\frac{M}{M_{\rm eq}}\right)^{4/3}(G\mu a)^2. \tag{61}$$

Numerically, we find

$$MN_{\rm acc}(a,M){\rm Mpc}_0^3 = 3.5\times 10^{24}\alpha_v\beta\delta\mathcal{P}\left(\frac{\alpha\mu_{-8}^2a^2}{\beta\alpha_v^2}\right)^{19/3}\left(\frac{M}{M_\odot}\right)^{-7}, \tag{62}$$

$$MN_{\rm norm}(a,M){\rm Mpc}_0^3 = 2\times 10^8\delta\mathcal{P}\frac{\alpha}{\alpha_v}a^2\mu_{-8}^2\left(\frac{M}{M_\odot}\right)^{-5/3}, \tag{63}$$

where the unit ${\rm Mpc}_0 = {\rm Mpc}/(1+z_{\rm eq})$ is the comoving length which is a megaparsec today. We plot these distributions in Figs. 2 and 3 for two different values of $G\mu$.

In the delta-function approximation for g, the largest contribution to the number density of halos is from the smallest loops (since their number density is larger). This is cut off when the resulting halos are too small to form stars. As we consider larger halos, we consider larger loops still in the normal growth regime. This is cut off when the loops are moving too fast

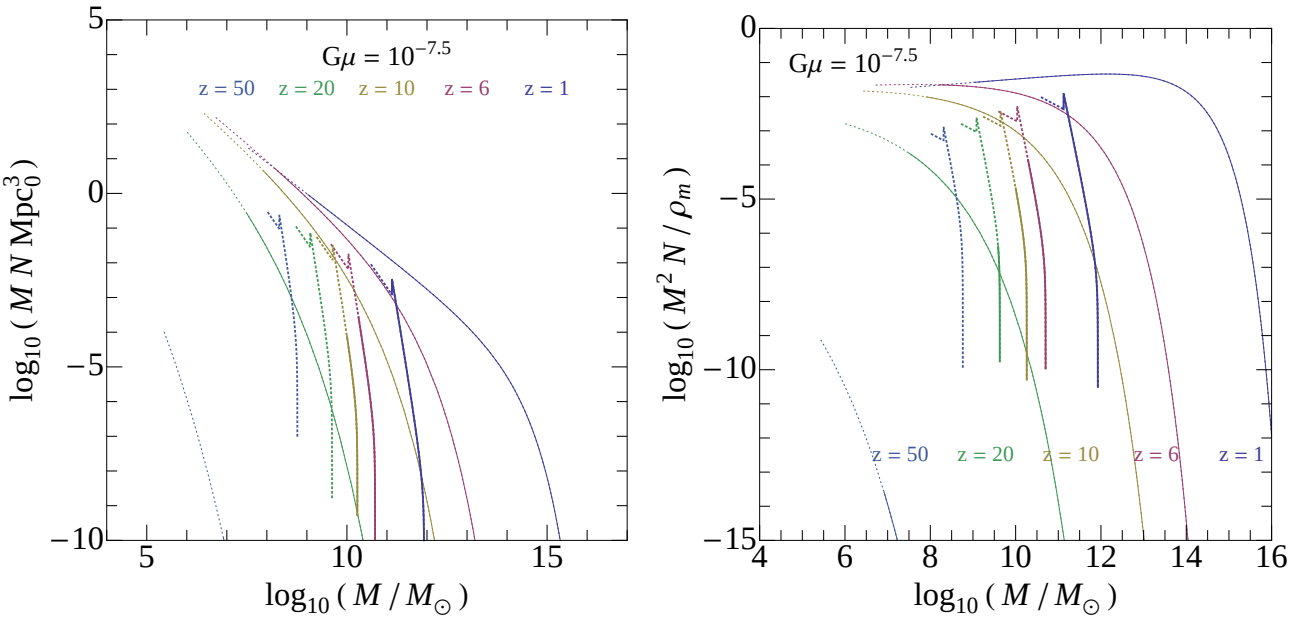

FIG. 2: Number and mass densities of halos per logarithmic mass bin. Solid lines indicate halos with $T_{\rm vir} > 10^4$K, and dotted lines extend this to 10^3K. The Sheth-Tormen mass function is used for comparison (thin lines). The delta-function approximation for g is used with $\alpha = 0.05$, $\alpha_v = 0.3$, and $\delta\mathcal{P} = 5$.

to be in the normal growth regime. Even larger loops are responsible for accelerated growth halos. The discontinuity in the graphs at the transition to this regime is caused by the discontinuity in the Jacobian factor $(\partial m/\partial M)$. The sharp decline of the halo distribution in the accelerated growth regime reflects the steep M^{-7} dependence in Eq. (62).

From the figures, there is a clear enhancement of early star formation provided $G\mu \gtrsim 10^{-7}$ if $T_* = 10^4$ K, and even for $G\mu \gtrsim 10^{-7.5}$ if $T_* = 10^3$ K. This enhancement occurs for redshifts $z \gtrsim 20$. Using our delta-function approximation for g, there is no early star formation for $G\mu \leq 10^{-8}\left(\frac{T_*}{10^4\text{K}}\right)$, although more precisely, the low momentum tail of g will produce some early stars.

V. BARYON COLLAPSE FRACTION

The fraction of baryons which collapse into stars is roughly equal to the fraction of matter in star-forming halos, i.e., those of sufficient virial temperature for efficient atomic hydrogen cooling. Because the process of filament collapse does not significantly affect the virial

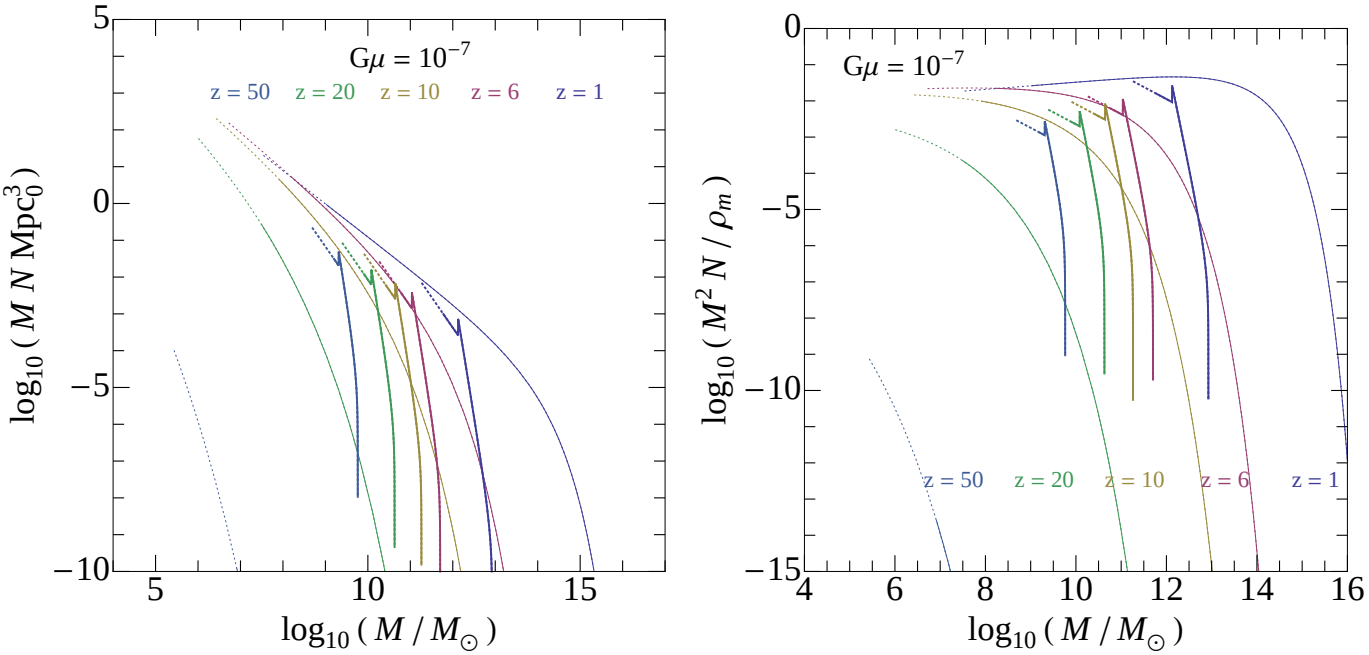

FIG. 3: Number density (left) and mass density (right) in halos with $T_{\rm vir} > 10^4$K (solid) and $T_{\rm vir} > 10^3$K (dotted) for higher tension strings.

temperature of the gas, we can neglect this process and simply count the fraction of matter in filaments of sufficient mass to form stars, i.e., those of mass $M_{\rm fil} \geq M^*_{\rm fil}$. The collapse fraction is

$$F_{\rm col} = \frac{1}{\rho_{\rm m}} \int_{M^*_{\rm fil}}^{\infty} dM_{\rm fil} M_{\rm fil} N_{\rm fil}(M_{\rm fil}), \tag{64}$$

$$= \frac{1}{\rho_{\rm m}} \int_{m_*}^{\infty} M_{\rm fil}(m) n(a_{\rm eq}, m, v_{\rm eq}) dm dv_{\rm eq}, \tag{65}$$

$$\approx 6\pi G t_{\rm eq}^2 \int_{m_*}^{\infty} M_{\rm fil}(m) \frac{\delta\mathcal{P}\mu^{3/2}\alpha^{1/2}}{2(2t_{\rm eq})^{3/2} m^{5/2}} dm, \tag{66}$$

$$\approx \frac{3\pi a G \delta\mathcal{P}\sqrt{t_{\rm eq}\alpha\mu^3}}{2\sqrt{2}} \left[\int_{\min\{m_*, m_{\rm acc}\}}^{m_{\rm acc}} \frac{dm}{m^{3/2}} + m_{\rm acc} \int_{\max\{m_*, m_{\rm acc}\}}^{\infty} \frac{dm}{m^{5/2}} \right], \tag{67}$$

where m_*, the smallest loop mass responsible for star forming filaments, is determined from $T_{\rm vir} \geq T_*$ and Eq. (36) to be

$$m_* = \frac{18 M_{\rm eq} T_*^2 \alpha_v^2}{G\mu\alpha m_p^2}. \tag{68}$$

The smallest loop mass undergoing accelerated growth is given by

$$m_{\rm acc} = \left(\frac{2\alpha a^2 G^5 \mu^5}{\beta^4 \alpha_v^2} \right)^{1/3} M_{\rm eq}. \tag{69}$$

The filament mass $M_{\rm fil}(m)$ from Eq. (33) then takes the form

$$M_{\rm fil}(m) = \begin{cases} am & m \leq m_{\rm acc} \\ am_{\rm acc} & m \geq m_{\rm acc}. \end{cases} \tag{70}$$

It will be convenient to define the time after which no star-forming filaments are in the normal-growth regime by $m_* = m_{\rm acc}$, yielding

$$a_* = \frac{54 T_*^3 \alpha_v^4 \beta^2}{G^4 \mu^4 m_p^3 \alpha^2}. \tag{71}$$

Then we can write

$$F_{\rm col} = \begin{cases} \dfrac{3\pi G a \delta \mathcal{P} \sqrt{t_{\rm eq} \alpha \mu^3}}{\sqrt{2}} \dfrac{m_{\rm acc}}{3 m_*^{3/2}} & a < a_* \\ \dfrac{3\pi G a \delta \mathcal{P} \sqrt{t_{\rm eq} \alpha \mu^3}}{\sqrt{2}} \left(\dfrac{1}{\sqrt{m_*}} - \dfrac{2}{3\sqrt{m_{\rm acc}}} \right) & a \geq a_*. \end{cases} \tag{72}$$

It is here where we could examine the consequences of using the delta-function approximation for the loop production function g. Notice that the low velocity tail of the distribution will rapidly diminish the value of $a_* \propto \alpha_v^4$. This means the second ($a > a_*$) part of Eq. (72) is relevant, and we see that the loop velocity dependence is $F_{\rm col} \propto 1/\alpha_v$, which is not steep enough to warrant concern that the delta-function approximation for g is bad.

VI. IONIZATION HISTORY

The fraction of volume which has been re-ionized is given by the baryon collapse fraction $F_{\rm col}$ as

$$Q_{\rm HII}(a) = \int_0^a \frac{N_{\rm ion}}{0.76} \frac{dF_{\rm col}}{da'} e^{F(a',a)} da', \tag{73}$$

where the number of ionizing photons per baryon is $N_{\rm ion} = 4000 f_\star f_{\rm esc} \approx 40$, where $f_\star \approx 1/10$ is the efficiency and $f_{\rm esc} \approx 1/10$ is the fraction which escape the halo. Here

$$F(a', a) = -0.26 \frac{C}{10} \left[\left(\frac{1 + z_{\rm eq}}{a'} \right)^{3/2} - \left(\frac{1 + z_{\rm eq}}{a} \right)^{3/2} \right], \tag{74}$$

with clumpiness $C \sim 1$. We can evaluate $Q_{\rm HII}(z)$ in closed form using the incomplete Gamma function, although the result is rather long, so we will not present it explicitly here. We plot

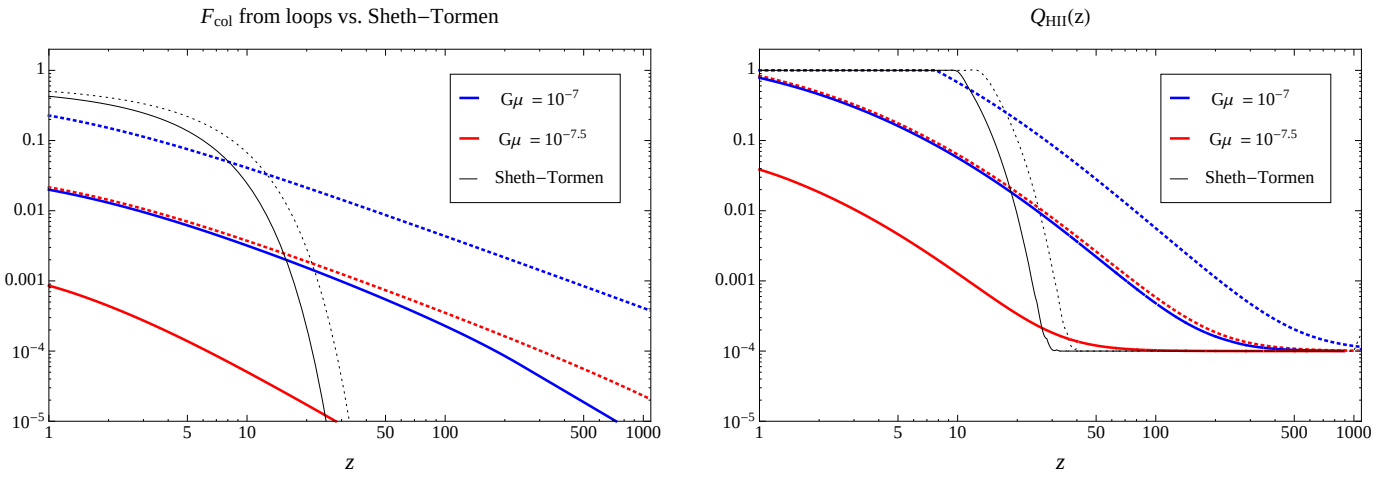

FIG. 4: Fraction of matter in star-forming halos (left) and fraction of volume which has been reionized (right) as a function of redshift. Dotted lines assume stars form in halos with $T_{\rm vir} > 10^3$K. We include a residual floor of 10^{-4} in $Q_{\rm HII}$.

$F_{\rm col}(z)$ and $Q_{\rm HII}(z)$ below using $N_{\rm ion} = 40$. **[Avi, you suggested this value before, but it seems to be ruled out by the graph in Fig.6. So, what value should we use?]**

We can find the optical depth by integrating the reionization fraction out to redshift z via

$$\tau(z) = \int_0^z n_{\rm H}(z') Q_{\rm HII}(z') \sigma_{\rm T} \frac{dz'}{(1+z')H(z')}, \tag{75}$$

where $n_{\rm H}(z)$ is the physical number density of hydrogen, equal to $2.7 \times 10^{-7}{\rm cm}^{-3}$ today, and $\sigma_{\rm T} = 6.652 \times 10^{-25}{\rm cm}^2$ is the Thomson cross-section. The Hubble rate obeys $H(z) = H_0\sqrt{\Omega_\Lambda + \Omega_m(1+z)^3}$, with $\Omega_\Lambda = 0.728$ and $\Omega_m = 1 - \Omega_\Lambda$. The visibility function $V(z)$ is defined through the optical depth τ via,

$$V(z) = e^{-\tau(z)} H(z) \frac{\partial \tau}{\partial z}. \tag{76}$$

Using the WMAP measured value of the reionization optical depth $\tau = 0.087 \pm 0.014$, we can find the excluded region of $N_{\rm ion}$-$G\mu$ parameter space, shown in Fig. 6 below.

VII. DISCUSSION

Loops of cosmic string can seed relatively massive halos at very early times. These halos can become sites of early star formation and can influence the ionization history of the

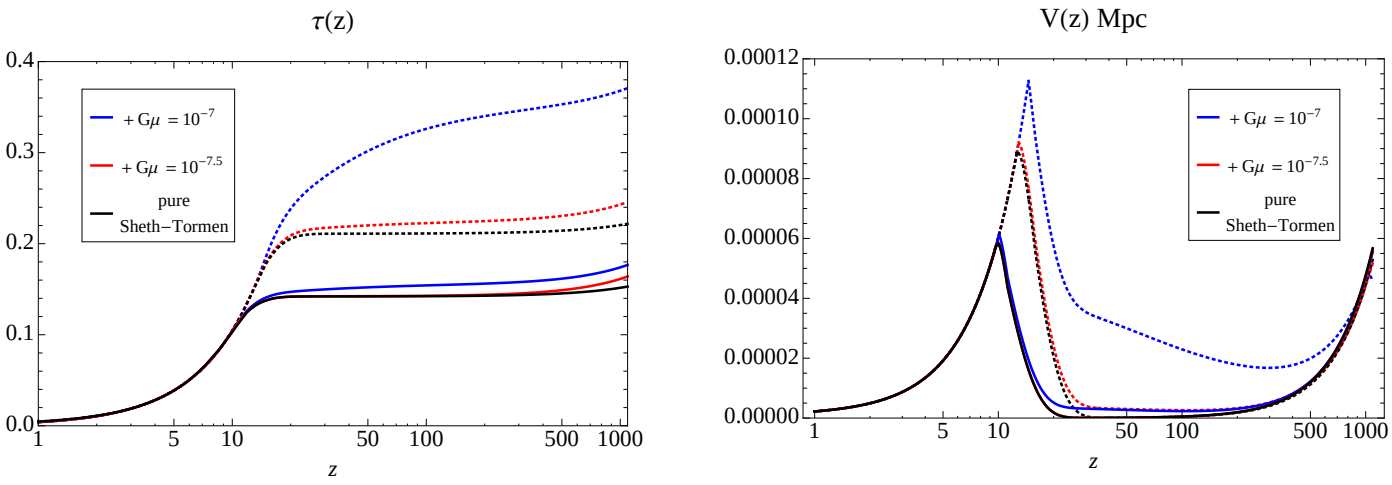

FIG. 5: Optical depth (left) and visibility function (right) for Sheth-Tormen plus cosmic strings. Dotted lines assume star formation from halos with $T_{\rm vir} > 10^3$K.

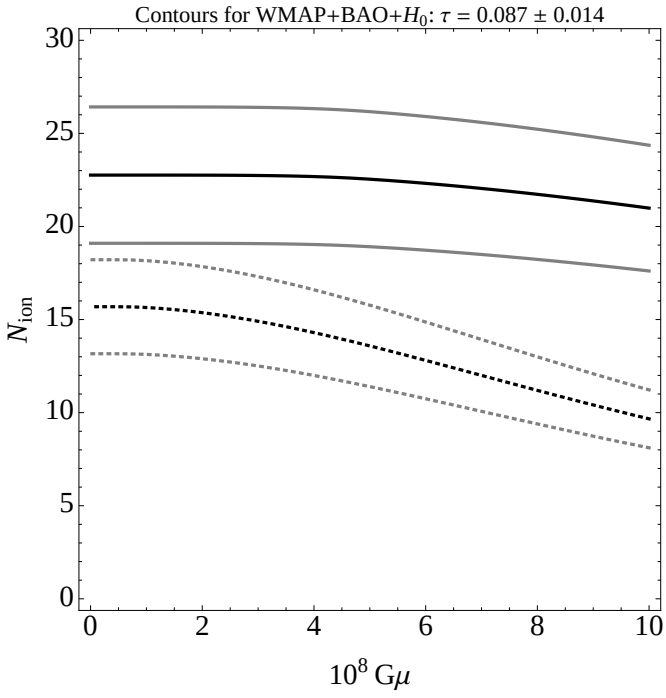

FIG. 6: Parameter space between the gray lines is compatible with the WMAP+BAO+H_0[41] reionization optical depth. The pure Sheth-Tormen scenario is equivalent to $G\mu = 0$. Dotted lines assume star formation from halos with $T_{\rm vir} > 10^3$K. Solid lines assume star formation from halos with $T_{\rm vir} > 10^4$K.

universe. With reasonable assumptions about the physics of reionization, the existence of strings is in conflict with the WMAP data, unless the string energy scale obeys the bound

[The following text needs to be updated; it refers to our earlier calculations.]

$$G\mu \lesssim 3 \times 10^{-8}. \tag{77}$$

This bound is an order of magnitude stronger than the current bounds based on the observation of CMB anisotropies [11–13]. As we mentioned in the Introduction, a stronger bound, $G\mu \lesssim 4\times10^{-9}$, was obtained from millisecond pulsar measurements in Ref. [14]. This bound, however, does not account for the fact that a significant fraction of the string network energy goes into the kinetic energy of loops, which is then redshifted. It also assumes that nearly all loops develop cusps, while examination of loops produced in the recent simulations suggests that cusps are rather rare [**?**]. Accounting for these effects is likely to relax the pulsar bound by an order of magnitude or so.

Acknowledgments

VIII. APPENDIX

A. The rocket effect

The gravitational radiation from a cosmic string loop is anisotropic in general. This affects the momentum of the loop. Let the radiation be beamed in the minus y-direction. The physical y-momentum $p = mv/\sqrt{1-v^2}$ of the loop then obeys

$$\frac{dp}{dt} = -Hp + \Gamma_{\rm P} G\mu^2, \tag{78}$$

where[3] $\Gamma_{\rm P} \sim 10$.

If we assume the non-relativistic loop has velocity $v_{\rm eq} > 0$ in the $+y$-direction at $t_{\rm eq}$, its subsequent velocity is given by

$$v(a) = \frac{v_{\rm eq}}{a} + \frac{3\Gamma_{\rm P} G\mu^2 t_{\rm eq}(a^{3/2} - a^{-1})}{5m}, \tag{79}$$

[3] This value was estimated for simple Kibble-Turok [42] loop solutions involving a few lowest harmonics. Recent simulations have shown that loops chopped off the network tend to be rectangular [43], which can suppress $\Gamma_{\rm P}$.

where $a = (t/t_{\rm eq})^{2/3}$. The trajectory in comoving coordinates is then

$$y(a) = \frac{9\Gamma_{\rm P} G\mu^2 t_{\rm eq}^2}{20m}\left(\frac{4}{\sqrt{a}} + a^2 - 5\right) + 3v_{\rm eq}t_{\rm eq}\left(1 - \frac{1}{\sqrt{a}}\right), \tag{80}$$

and so the matter-era velocity of the loop formed at a_i in the radiation era is

$$v(a, a_i) = \alpha_v \frac{a_i}{a} + \frac{(1 + 9a^{5/2} - 10a_i^3)\Gamma_{\rm P} G\mu}{30aa_i^2\alpha} \approx \alpha_v \frac{a_i}{a} + \frac{3a^{3/2}\Gamma_{\rm P} G\mu}{10a_i^2\alpha}. \tag{81}$$

From this, we can calculate the turnaround surfaces, and find the average filament thickness by

$$\langle x_{\rm ta}^2 \rangle = \frac{\int x_{\rm ta}^4(y)dy}{\int x_{\rm ta}^2(y)dy}, \tag{82}$$

which determines the average bead mass found in Sec. III E. For filaments from loops produced after $a_i \sim 0.02\mu_{-8}$, this leads to a correction factor of order 0.8 to the average filament radius. The only loops whose filaments receive significant corrections from the rocket effect are those whose number-densities are highly suppressed due to loop evaporation. Loop evaporation becomes significant only for loops of mass below

$$m_\Gamma = \Gamma G\mu^2 t_{\rm eq}. \tag{83}$$

Since no star formation results from loops of mass less than m_* given by Eq.(68), we can neglect loop evaporation for

$$\frac{9T_*^2\alpha_v^2}{25G^3\mu^3\alpha m_p^2} \leq 1, \tag{84}$$

i.e.,

$$\mu_{-8} \lesssim 80\left(\frac{T_*}{10^4{\rm K}}\right)^{2/3} \gtrsim 20. \tag{85}$$

For this reason, we can neglect loop evaporation and the rocket effect entirely.

---

[1] T.W.B. Kibble, J. Phys. **A9**, 1387 (1976).

[2] S. Sarangi, S. H. H. Tye, "Cosmic string production towards the end of brane inflation," Phys. Lett. **B536**, 185-192 (2002). [hep-th/0204074];

[3] G. Dvali and A. Vilenkin, JCAP **0403**, 010 (2004).

[4] E.J. Copeland, R.C. Myers and J. Polchinski, JHEP **0406**, 013 (2004).

[5] A. Vilenkin, "Cosmic Strings As Gravitational Lenses," Astrophys. J. **282**, L51 (1984).

[6] B. Shlaer and S. -H. H. Tye, "Cosmic string lensing and closed time-like curves," Phys. Rev. D **72**, 043532 (2005) [hep-th/0502242].

[7] B. Shlaer and M. Wyman, "Cosmic superstring gravitational lensing phenomena: Predictions for networks of (p,q) strings," Phys. Rev. D **72**, 123504 (2005) [hep-th/0509177].

[8] N. Kaiser and A. Stebbins, "Microwave Anisotropy Due to Cosmic Strings," Nature **310**, 391 (1984).

[9] A. Vilenkin and E. P. S. Shellard, *Cosmic Strings and Other Topological Defects*, Cambridge University Press, Cambridge, England, (1994).

[10] E.J. Copeland, L. Pogosian and T. Vachaspati, arXiv:1105.0207 [hep-th].

[11] M. Wyman, L. Pogosian, I. Wasserman, "Bounds on cosmic strings from WMAP and SDSS," Phys. Rev. **D72**, 023513 (2005). [astro-ph/0503364].

[12] R. Battye and A. Moss, arXiv:1005.0479 [astro-ph].

[13] C. Dvorkin, M. Wyman and W. Hu, arXiv:1109.4947 [astro-ph].

[14] R. van Haasteren, Y. Levin, G. H. Janssen, K. Lazaridis, M. K. B. W. Stappers, G. Desvignes, M. B. Purver, A. G. Lyne *et al.*, "Placing limits on the stochastic gravitational-wave background using European Pulsar Timing Array data," [arXiv:1103.0576 [astro-ph.CO]].

[15] M.J. Rees, MNRAS **222**, 27 (1986).

[16] T. Hara, P. Mahonen and S. Miyoshi, Ap. J. **412**, 22 (1993).

[17] P.P. Avelino and A.R. Liddle, MNRAS **348**, 105 (2004).

[18] L. Pogosian, A. Vilenkin, "Early reionization by cosmic strings revisited," Phys. Rev. **D70**, 063523 (2004). [astro-ph/0405606].

[19] K. D. Olum, A. Vilenkin, "Reionization from cosmic string loops," Phys. Rev. **D74**, 063516 (2006). [astro-ph/0605465].

[20] D. P. Bennett, F. R. Bouchet, "Evidence for a Scaling Solution in Cosmic String Evolution," Phys. Rev. Lett. **60**, 257 (1988); Phys. Rev. Lett. **63**, 2776 (1989).

[21] B. Allen and E.P.S. Shellard, Phys. Rev. Lett. **64**, 119 (1990).

[22] V. Vanchurin, K. D. Olum, A. Vilenkin, "Scaling of cosmic string loops," Phys. Rev. **D74**, 063527 (2006). [gr-qc/0511159].

[23] K. D. Olum, V. Vanchurin, "Cosmic string loops in the expanding Universe," Phys. Rev. **D75**,

063521 (2007). [astro-ph/0610419].

[24] J. J. Blanco-Pillado, K. D. Olum, B. Shlaer, "Large parallel cosmic string simulations: New results on loop production," Phys. Rev. **D83**, 083514 (2011). [arXiv:1101.5173 [astro-ph.CO]].

[25] A. Vilenkin, "Cosmological Density Fluctuations Produced by Vacuum Strings," Phys. Rev. Lett. **46**, 1169-1172 (1981).

[26] A. Albrecht, N. Turok, "Evolution of Cosmic Strings," Phys. Rev. Lett. **54**, 1868-1871 (1985).

[27] M.G. Jackson, N.T. Jones and J. Polchinski, JHEP **0510**, 013 (2005).

[28] T. Damour and A. Vilenkin, Phys. Rev. **D71**, 063510 (2005).

[29] M. Sakellariadou, JCAP **0504**, 003 (2005).

[30] A. Avgoustidis and E.P.S. Shellard, Phys. Rev. **D71**, 123513 (2005).

[31] F. Dubath, J. Polchinski and J.V. Rocha, Phys. Rev. **D77**, 123528 (2008).

[32] A. Loeb, *How Did the First Stars and Galaxies Form?*, Princeton University Press, Princeton, NJ, U.S.A., (2010)

[33] A. Stacy, V. Bromm, A. Loeb, "Effect of Streaming Motion of Baryons Relative to Dark Matter on the Formation of the First Stars," [arXiv:1011.4512 [astro-ph.CO]].

[34] D. Tseliakhovich, R. Barkana, C. Hirata, "Suppression and Spatial Variation of Early Galaxies and Minihalos," [arXiv:1012.2574 [astro-ph.CO]].

[35] E. Bertschinger, "Cosmological accretion wakes," Astrophys. J. **316**, 489 (1987).

[36] A. C. Quillen, J. Comparetta, "Jeans Instability of Palomar 5's Tidal Tail," [arXiv:1002.4870 [astro-ph.CO]].

[37] O. F. Hernandez, Y. Wang, R. Brandenberger, J. Fong, "Angular 21 cm Power Spectrum of a Scaling Distribution of Cosmic String Wakes," [arXiv:1104.3337 [astro-ph.CO]].

[38] V. Zanchin, J. A. S. Lima, R. H. Brandenberger, "Accretion of cold and hot dark matter onto cosmic string filaments," Phys. Rev. **D54**, 7129-7137 (1996). [astro-ph/9607062].

[39] R. K. Sheth, G. Tormen, "Large scale bias and the peak background split," Mon. Not. Roy. Astron. Soc. **308**, 119 (1999). [astro-ph/9901122].

[40] D. J. Eisenstein, A. Loeb, E. L. Turner, "Dynamical mass estimates of large scale filaments in redshift surveys," Submitted to: Astrophys. J.. [astro-ph/9605126].

[41] N. Jarosik, C. L. Bennett, J. Dunkley, B. Gold, M. R. Greason, M. Halpern, R. S. Hill, G. Hinshaw *et al.*, "Seven-Year Wilkinson Microwave Anisotropy Probe (WMAP) Observations: Sky Maps, Systematic Errors, and Basic Results," Astrophys. J. Suppl. **192**, 14 (2011).

[arXiv:1001.4744 [astro-ph.CO]].

[42] T.W.B. Kibble and N.G. Turok, Phys. Lett. ??

[43] C. J. Copi, T. Vachaspati, "Shape of Cosmic String Loops," Phys. Rev. **D83**, 023529 (2011). [arXiv:1010.4030 [hep-th]].